Direct observation and theoretical study of cavitation bubbles in liquid mercury

Masato Ida*
Center for Computational Science and E-systems, Japan Atomic Energy Agency, 6-9-3 Higashi-Ueno, Taito-ku, Tokyo 110-0015, Japan

Takashi Naoe
Graduate School of Science and Engineering, Ibaraki University, Hitachi-shi, Ibaraki-ken 316-851, Japan

Masatoshi Futakawa
Quantum Beam Science Directorate, Japan Atomic Energy Agency, Tokai-mura, Ibaraki-ken 319-1195, Japan
(Received 17 October 2006; published 12 April 2007)

The direct observation of cavitation bubbles emerging in liquid mercury under the action of mechanical impacts and theoretical investigations on the experimental results have been made. Through a glass wall, the image of cavitation bubbles appearing near or in contact with the wall was captured by high-speed cameras. Discrepancies found between the bubbles' growth rates determined experimentally and given by a single-bubble theory have been discussed using a theoretical model of Rayleigh-Plesset type that takes into account bubble-bubble and bubble-wall interactions. A theoretical equation for the asymptotic growth rate in a multibubble case has been given and time dependence of the growth rate under a constant negative pressure has been clarified.

DOI: 10.1103/PhysRevE.75.046304 PACS number(s): 47.55.dp, 47.55.dd

I. INTRODUCTION

Cavitation in fluid machinery has been a serious issue in many hydraulic applications, causing erosion of solid surfaces and resulting sometimes in destruction of structures. Such a problem can also be found in high-power spallation neutron sources, in which liquid mercury is used as the spallation target material (and also as a coolant) [1–3]. In a series of test experiments (see, e.g., Refs. [1–5]), it has been suggested that intense pressure waves produced by proton spallation reactions in the mercury target should lead to cavitation in liquid mercury, which results in erosion of the target vessel caused by violent collapse of cavitation bubbles and will seriously shorten the target lifetime (the current estimation of the lifetime is about 30 hours which is much shorter than the previously predicted value, 2500 hours, determined by radiation embrittlement [6]). To overcome this issue, research groups in the Japan Atomic Energy Agency (formerly the Japan Atomic Energy Research Institute) and the Oak Ridge National Laboratory have been performing various experimental (both in-beam and off-line) and theoretical investigations.

In this paper, we report the direct observation of cavitation bubbles emerging in liquid mercury, which is a conclusive evidence of the occurrence of cavitation, and perform theoretical investigations to understand the experimental results. Although the previous experiments have provided indirect evidences of cavitation (e.g., pitting damages on metal plates and strong acoustic pulses probably induced by the collapse of bubbles), no direct observation has been achieved so far. In order to resolve this lack of direct evidence, we have performed an experimental study using a magnetically driven impact test device, called MIMTM (Magnetic IMpact Testing Machine) [4], and high-speed cameras [7]. In the experimental system, cavitation is induced by mechanical impacts on the mercury container, which produce a negative pressure in liquid mercury. One serious difficulty in the direct observation of cavitation bubbles in liquid mercury comes from the opacity of liquid mercury. As is commonly known, liquid mercury is an opaque liquid and thus makes it impossible for one to see through what takes place inside (probably because of this difficulty, only a very few studies have been made previously on cavitation in liquid mercury [8,9]). We overcame this difficulty by a rather primitive approach, setting a glass window on the upper side of the mercury container. The image of cavitation bubbles appearing near, or in contact with, the glass window was captured by high-speed cameras. Theoretical discussions on the experimental results are given by using a system of equations of Rayleigh-Plesset type, and attempts are made to explain noticeable discrepancies found between the experimental and theoretical values of the growth rate of bubbles. Bubble-bubble and bubble-wall interactions under a constant negative pressure were the main concerns in the theoretical investigation. Time dependence of the growth rate due to the interactions has been clarified theoretically. In this paper we mainly give a qualitative discussion since there must be significant experimental uncertainties much larger than in the case of water that resulted from the opacity and are unavoidable at present.

In Sec. II the experimental setup is illustrated and the experimental results are presented. In Sec. III theoretical investigations on the experimental results are given focusing on the growth rate of cavitation bubbles. Section IV summarizes the present paper.

II. EXPERIMENT

Figure 1 illustrates the experimental setup when the pressure inside the mercury is measured. The body of the

*Electronic address: ida.masato@jaea.go.jp

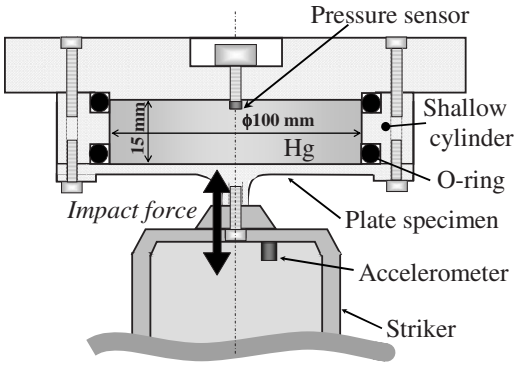

FIG. 1. Experimental setup when the pressure inside the mercury is measured. The shallow cylinder filled with liquid mercury is the main body of the MIMTM system. The mechanical impacts are imposed from the bottom by electromagnetic force.

MIMTM system is a shallow cylinder made of stainless steel, filled with liquid mercury (not degassed) of about 120 cc. Mechanical impacts are imposed on the mercury from the bottom of the cylinder by a magnetic coil whose output can be controlled by changing the electric current. The pressure change inside the cylinder is measured using a pressure sensor (Entran® EPXH) attached on the upper panel of the cylinder. Figure 2 shows the pressure profile for an input power of 560 W recorded at a sampling rate of 50 kHz. After a rapid decrease, the pressure appears to be in a saturated state at about −0.123 MPa lasting for about 1 ms, which is followed by strong (positive) pressure pulses. To investigate in detail what happened during this period, we have attempted to observe the inside of the mercury through a glass window embedded in the upper panel; see Fig. 3 for the experimental setup for image recording. We used two kinds of high-speed cameras; one is a high-speed shutter camera (NAC, DiCAM PRO) which allows us to take clear, high-resolution images, and the other is a high-speed video camera (NAC, Memrecam fx RX6) which is used to take high-frame-rate, but rather low-resolution, movies of dynamical behaviors.

Photographic series of the recorded phenomenon are shown in Figs. 4 and 5. Figure 4 shows the high-resolution images at time=0.5 ms and 1.7 ms measured from the time

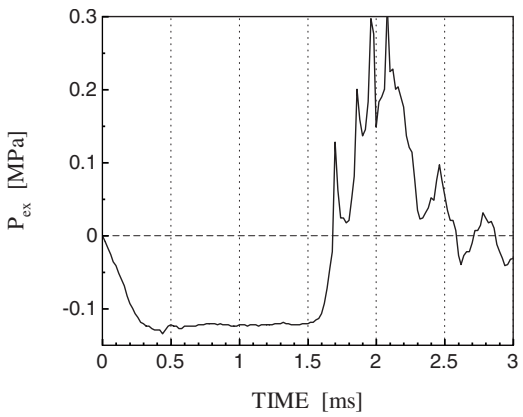

FIG. 2. Pressure change inside the mercury generated by a single mechanical impact.

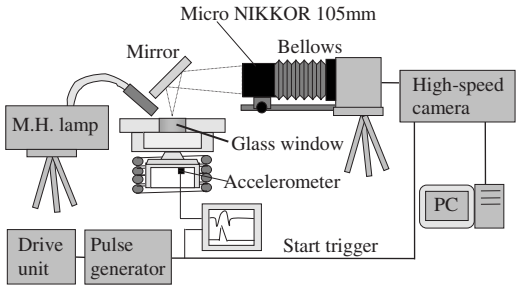

FIG. 3. Experimental setup when the bubble behavior is observed. The pressure sensor in Fig. 1 is replaced with a glass window, through which the mercury surface is monitored. The image is recorded by a high-speed camera (a high-speed shutter camera or a high-speed video camera) through a mirror.

when a mechanical impact was imposed, and Fig. 5 shows three series of cutout images at three different locations taken from the movie. Many spherical cavities expanding and then rapidly shrinking can be seen clearly in the liquid mercury, some of which experienced mutual coalescence as shown in the lowest series of Fig. 5. They must be bubbles that emerged through cavitation caused by the negative pressure. The bubbles were expanding when the absolute pressure (the atmospheric pressure plus the pressure change

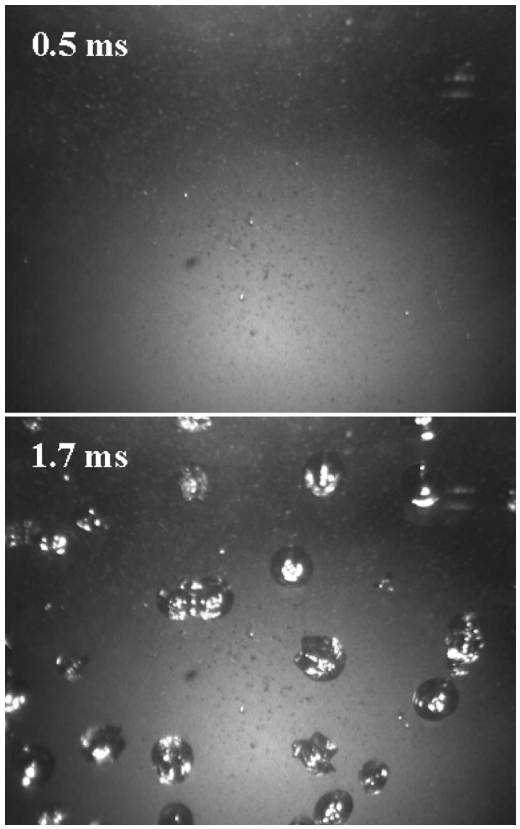

FIG. 4. High-resolution images of the mercury surface captured by a high-speed shutter camera through a glass window. The observation was made at 0.5 ms and 1.7 ms after imposing the impact. The width of the panels correspond to 13 mm. Many cavities can be seen, which must be cavitation bubbles. The average distance between nearby bubbles is a few millimeters.

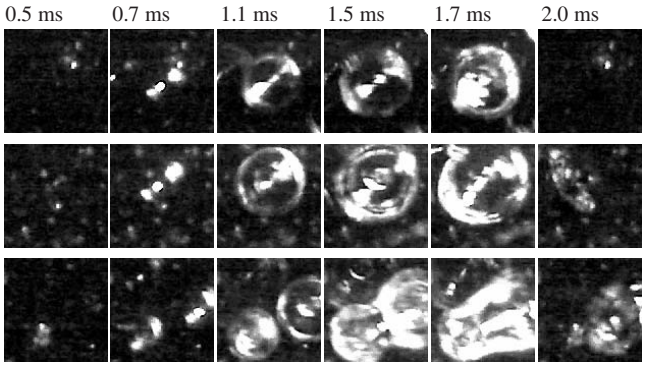

FIG. 5. Time sequences of the images of the mercury surface at three different locations, captured by a high-speed video camera. The width of the frames corresponds to 1 mm. The radius change of the bubbles can be deduced from this series of images. The two bubbles shown in the lowest series experienced mutual coalescence during the expansion phase.

shown in Fig. 2) was negative, and then collapsed away or disappeared from our sight at around 2 ms. The growth rate of the bubbles, i.e., the time derivative of the bubbles' radii, deduced from the captured pictures is on the order of 1 m/s, and their lifetime, the time period where the bubbles are visible, is about 1.5 ms. The collapse time of the bubbles is well correlated with the time when the strong pressure pulses were detected, an observation which may prove that the pulses were emitted by the bubble collapse.

III. THEORETICAL INVESTIGATIONS

We have performed theoretical investigations on the growth rate and maximum size of the observed bubbles, both of which should have a strong correlation with the erosion intensity that the bubbles will have. We have not discussed the collapse phase since it was unfortunately not clearly recorded particularly during the period where the bubbles were very small. The theoretical model used in the present study is a Rayleigh-Plesset equation involving a term that represents bubble-bubble (or, in some cases, bubble-wall) interaction,

$$R_i\ddot{R}_i + \frac{3}{2}\dot{R}_i^2 - \frac{p_{m\,i}}{\rho} = -\frac{p_{\mathrm{ex}}(t)}{\rho} - \sum_{j=1,j\neq i}^{N} \frac{1}{r_{ij}}\frac{d(R_j^2\dot{R}_j)}{dt}, \quad (1)$$

$$p_{m\,i} = p_v + \left(P_0 + \frac{2\sigma}{R_{i0}}\right)\left(\frac{R_{i0}}{R_i}\right)^{3\kappa} - \frac{2\sigma}{R_i} - \frac{4\mu}{R_i}\dot{R}_i - P_0, \quad (2)$$

where R_i is the time dependent radius of bubble i, $p_{\mathrm{ex}}(t)$ is the driving pressure, ρ is the density of liquid mercury, r_{ij} is the distance between the centers of bubbles i and j, p_v is the vapor pressure, P_0 is the atmospheric pressure, σ is the surface tension, R_{i0} is the equilibrium radius of bubble i, and μ is the viscosity of liquid mercury. This system of equations governs the forced volume oscillation of N spherical bubbles interacting with each other through sound (see, e.g., Refs. [10–13] for recent studies using this kind of theoretical model). The last term of Eq. (1) denotes the pressure of the sounds emitted by the other bubbles measured at the position of bubble i, representing bubble-bubble interaction through sound. Bubble-bubble interaction in a sound field is known to alter the physical properties of bubbles in diverse ways (see, e.g., Refs. [10–12,14–18] for recent studies), and hence we have examined its effects on the behavior of cavitation bubbles in liquid mercury. In the theoretical model, the surrounding liquid is assumed to be incompressible, which holds well in the expansion phase of the present case because the growth rate ($\approx$1 m/s) is much smaller than the sound velocity of liquid mercury (1450 m/s at room temperature).

The bubble dynamics in single-bubble cases (i.e., for $r_{ij} \to \infty$) predicted theoretically is shown in Figs. 6(b) and 6(c) by solid curves. Here, the recorded data shown in Fig. 2 was used for $p_{\mathrm{ex}}(t)$, and seven different initial radii were assumed as the equilibrium size of cavitation bubbles is in general not known. The other parameters used are $\rho=13\,528$ kg/m^3, $p_v=0.28$ Pa (negligibly small compared to P_0 and $-\min[P_0+p_{\mathrm{ex}}(t)]$), $P_0=0.1013$ MPa, $\sigma=0.47$ N/m, $\kappa=1$, and $\mu=1.52\times10^{-3}$ Pa s. For $R_{i0}\geqslant 9.2$ μm and $R_{i0}=8.95$ μm, rapid, unbounded growth of the bubbles is observed during the negative-pressure period, whereas for $R_{i0}=8.5$ μm and 9 μm an oscillatory behavior probably centered at the equilibrium radius for the negative pressure can be seen. The latter case, which corresponds to the situation where the bubble radius does not exceed the (dynamic) Blake critical radius, exhibits a completely different behavior from that of the experimentally observed bubbles and is thus not discussed further in this paper.

Significant qualitative and quantitative differences are found between the experimental observations (the symbols in Fig. 6) and theoretical results, though they are in reasonable agreement with each other in some respects. The growth rate and maximum radius in the experiment are considerably smaller than the theoretical ones, while the lifetime shows a reasonable agreement between experiment and theory. Also, the growth rate in the experiment appears to be time dependent, while the theoretical one seems to converge to an almost constant value after the transient has decayed. There are several possible factors causing the discrepancies. One comes from the opacity of liquid mercury, which must lead to significant uncertainties in optical observations; there is a possibility, for example, that the bubbles' main body greater than the observed circles is hidden by the mercury veils covering the surface of the glass window. Also, physical effects that are not taken into consideration in the theory (e.g., evaporation and condensation, gas diffusion, or some other effect) could be the origin of the discrepancies. Furthermore, bubble-bubble and bubble-wall interactions must have a considerable influence on the bubbles' dynamics because in the experiments many bubbles emerged simultaneously in the proximity of a glass wall. In what follows, in order to clarify as much as possible the origin of the discrepancies, we discuss the last factor by employing Eq. (1).

Though Eq. (1) is a model equation for spherical bubbles in an unbounded domain, it is, under some assumptions, also applicable to other configurations. In the present study we consider two cases: a case of spherical bubbles staying near a wall and a case of hemispherical bubbles located on a wall. Since the problems can be transformed into the interaction of spherical bubbles in an unbounded domain, both cases can

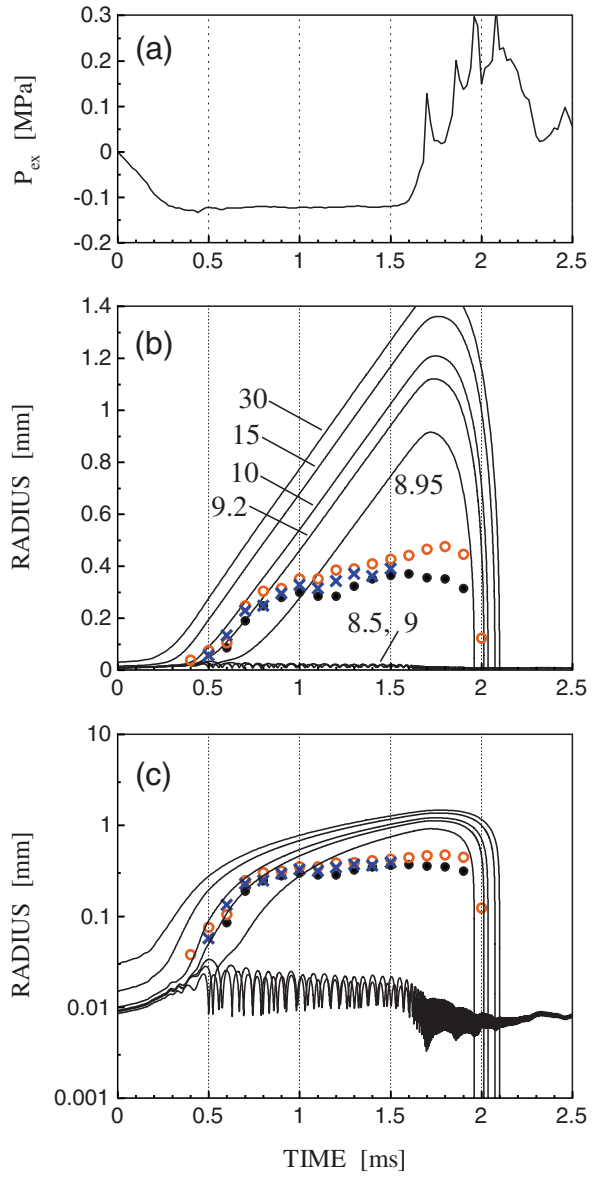

FIG. 6. (Color online) Experimental and numerical results: the pressure change (a) and the bubble radii given experimentally (symbols) and numerically using a single-bubble model (lines) [(b) in linear scale and (c) in log scale] as functions of time. The numbers presented in panel (b) denote the equilibrium radii (μm) assumed in the numerical study. The three sets of experimental data shown were taken from the recorded images. The bubble denoted by the crosses collided with a neighboring bubble at about 1.5 ms.

be addressed with Eq. (1). Assuming that the glass wall is flat and rigid and the sound reflection at the glass surface is in-phase, due to the mirror effect of the wall [18] the interaction between a spherical bubble and the nearby wall can be approximately transformed into the interaction of two identical bubbles in an unbounded domain oscillating in-phase with each other, separated by 2 times the distance between the bubble center and the wall surface. Hemispherical bubbles on the wall in the present case, as suggested by Bremond *et al.* in a study of cavitation in water [13], may be treated as spherical bubbles in an unbounded domain, because the maximum thickness of the viscous boundary layer formed on the wall surface in the expansion phase [$\sim$0.01 mm, estimated by $(\mu t_e/\rho)^{1/2}$ with t_e=1 ms] is much smaller than the maximum bubble radii and hence the wall only acts as a mirror. These problem transformations allow us to use a single theoretical model [Eq. (1)] to analyze both cases. Though we only present results for the former case below, they can also be regarded as results for the latter case: a case of two spherical bubbles near the wall, for example, is equivalent to a case of four hemispherical bubbles on the wall. (In a future study the model would be used to investigate more complex cases such as the interaction of bubbles on the wall with bubbles in the bulk of liquid mercury.)

Let us consider the dynamics of spherical bubbles near the glass wall. Assuming that the distance between the center of bubble i and the wall is D_i and, for simplicity, all D_i have the same value equal to D, Eq. (1) is rewritten into

$$R_i\ddot{R}_i + \frac{3}{2}\dot{R}_i^2 - \frac{p_{m\,i}}{\rho} = -\frac{p_{\rm ex}}{\rho} - \frac{1}{2D}\frac{d(R_i^2\dot{R}_i)}{dt} - \sum_{j=1,j\neq i}^{N}\left(\frac{1}{r_{ij}} + \frac{1}{s_{ij}}\right)\frac{d(R_j^2\dot{R}_j)}{dt}, \quad (3)$$

where $s_{ij}=(r_{ij}^2+4D^2)^{1/2}$ is the distance between the centers of bubble i and the mirror image of bubble j. The second term and the last term, respectively, on the right-hand side denote the amplitudes of the sounds emitted by the mirror image of bubble i and by bubble j and its mirror image. The radius-time curves for N=2 determined by Eq. (3) are shown in Fig. 7. In all cases shown in the figure, the maximum radii are remarkably decreased by the bubble-bubble and bubble-wall interactions and hence the numerical results become closer to the experimental ones. Interestingly, the explosive expansion of the bubble with an equilibrium radius of 9.2 μm observed in Fig. 6(b) was suppressed by the larger neighboring bubble; see Fig. 7(c). This may be caused by the positive pressure from the neighboring bubble, which enlarges the effective critical radius. The lifetime of the explosively expanding bubbles is slightly extended by the interactions, a result which is consistent with the previous experimental observations on bubble-wall interaction (see, e.g., Ref. [19]).

We have further discussed the growth rate to obtain a simple theoretical estimation of it in a multibubble case. In the experimental observation, the absolute pressure showed such a characteristic pattern that it held at a negative constant for about 1.2 ms. In the following, we thus study bubble dynamics in a constant negative pressure. Let us consider a case of two identical bubbles, that is, the case of $R_{10}=R_{20}$ and $R_1=R_2$ with N=2. Assuming that $p_{\rm ex}$ is a negative constant and $\ddot{R}_1 \approx 0$ or, in other words, all the force terms are approximately balanced, Eq. (3) is reduced to

$$\left[\frac{3}{2} + \left(\frac{1}{D} + \frac{2}{r_{12}} + \frac{2}{s_{12}}\right)R_1\right]\dot{R}_1^2 - \frac{p_{m1}}{\rho} = -\frac{p_{\rm ex}}{\rho}. \quad (4)$$

For $R_1 \gg R_{10}$, this equation gives the asymptotic growth rate in a multibubble case,

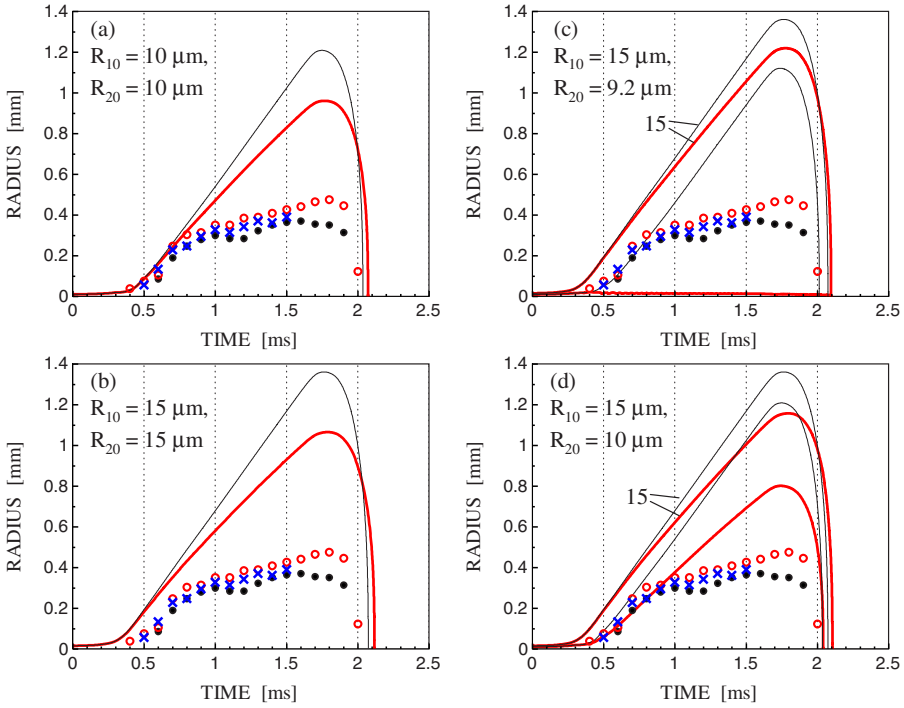

FIG. 7. (Color online) Effects of bubble-bubble and bubble-wall interactions in cases of two spherical bubbles near the glass wall. The thin and thick lines denote the numerical results for isolated and interacting bubbles, respectively, given by solving the coupled Rayleigh-Plesset equations, and the symbols denote the experimental results already shown in Fig. 6. Here, we assumed $D=1.2$ mm and $r_{12}=2$ mm with four different couples of equilibrium radii as indicated in the panels. As described in the text, the example considered here is approximately equivalent to a case of four hemispherical bubbles (two couples of identical hemispherical bubbles) on the wall.

$$\dot{R}_1 = \sqrt{\frac{p_v - P_0 - p_{\mathrm{ex}}}{\left[\frac{3}{2} + \left(\frac{1}{D} + \frac{2}{r_{12}} + \frac{2}{s_{12}}\right)R_1\right]\rho}}. \tag{5}$$

When the separation distances are infinite, this equation converges to

$$\dot{R}_1 = \sqrt{\frac{p_v - P_0 - p_{\mathrm{ex}}}{\frac{3}{2}\rho}}, \tag{6}$$

which is the asymptotic growth rate in single-bubble cases given previously [20]. From Eqs. (5) and (6) one can see that both the bubble-bubble and bubble-wall interactions reduces the growth rate, and the asymptotic growth rate in multibubble cases depends on the instantaneous radius while it is not radius dependent in single-bubble cases; actually, the lines in Fig. 7 for the interacting cases are slightly curved even in the constant-pressure period. (The same tendencies are also found when the bubbles have different radii; see the Appendix.) This radius dependence is interpreted as follows: in multibubble cases the amplitude of the total driving sound acting on a bubble is time dependent even if p_{ex} is constant because the amplitudes of the sounds emitted by the neighboring expanding bubbles are time dependent [note that $d(R_j^2\dot{R}_j)/dt = 2R_j\dot{R}_j^2 + R_j^2\ddot{R}_j$ in Eqs. (1) and (3) is not constant even for $\ddot{R}_j = 0$], and hence the bubbles in multibubble cases cannot be in steady growth. These theoretical results reproduce well the qualitative natures of the experimental result.

Last, we have performed a comparative study to confirm the quantitative accuracy of Eq. (5). The solid curves in Fig. 8 show the bubble radii and growth rates for $R_{10}=R_{20}=10$ μm determined numerically by solving Eq. (3). Here, the pressure change was idealized as $p_{\mathrm{ex}}=0$ MPa for $t<0$ s and $p_{\mathrm{ex}}=-0.123$ MPa for $t\geqslant 0$ s, and the radius and growth rate of an isolated bubble are also shown for reference. The dashed curves denote the asymptotic growth rates given by Eqs. (5) and (6) with the bubble radii determined numerically shown in the upper panel. This figure clearly shows the noticeable difference in the growth rates of isolated and interacting bubbles. The asymptotic values are in reasonable quantitative agreement with the full numerical solutions, proving that the theory accurately describes the characteristics of the explosively expanding bubbles, e.g., the remarkable decrease of the growth rate due to bubble-bubble and bubble-wall interactions.

IV. CONCLUSION

In summary, we have reported the direct observation of cavitation bubbles in liquid mercury, which was enabled using a glass window. The present experimental result offers a conclusive evidence of the occurrence of cavitation in liquid mercury. The theoretical investigations taking into account bubble-bubble and bubble-wall interactions have partly explained the qualitative and quantitative discrepancies found between the observed data and a single-bubble theory, i.e., the time dependence of the growth rate in experiment and its

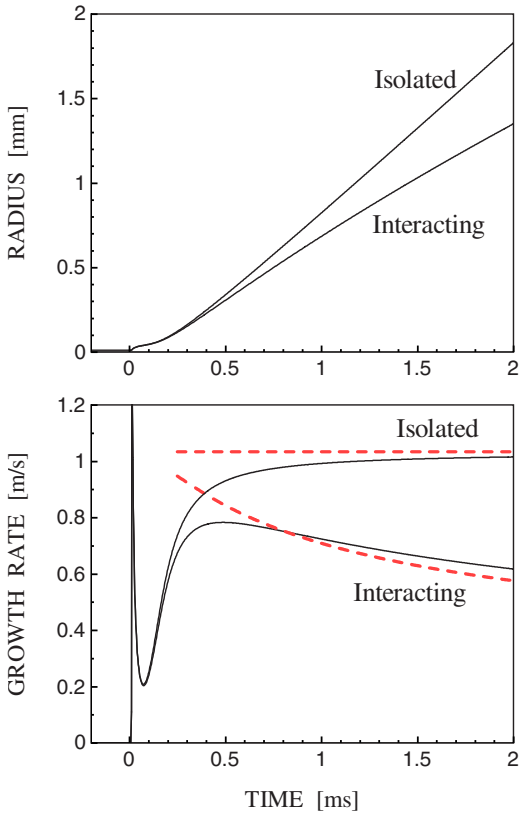

FIG. 8. (Color online) Asymptotic behavior of the growth rate under a constant negative pressure. Shown are the radii (the upper panel) and the growth rates (the lower panel) of isolated and two interacting bubbles for $R_{10}=R_{20}=10\ \mu$m given by solving the coupled Rayleigh-Plesset equations (the solid lines) and the corresponding asymptotic growth rates given by Eq. (5) (the dashed lines). Here the separation distances were assumed as in Fig. 7.

lower value than that given by the single-bubble theory. Those observations and findings would be fundamental knowledge for high-power pulse spallation neutron sources using a liquid metal such as the J-PARC (Japan Proton Accelerator Research Complex). However, further discussion is absolutely needed to clarify, in particular, the effects of experimental uncertainties coming from mercury's opacity, which have never been confronted in the previous experiments with water. We still have many unknowns resulting from the experimental difficulty, such as the actual three-dimensional shape of the cavitation bubbles, the macroscale structure of the cavitation field, and the matter whether other bubbles exist over the visible bubbles. Improving the experimental technique to achieve a finer observation of cavitation bubbles in such an opaque liquid would be a challenging task. Also, refining the theory by considering the interaction effects of a larger number of bubbles, including those in the bulk of the mercury, would be necessary to provide a quantitatively accurate prediction.

ACKNOWLEDGMENTS

This work was partly supported by the Ministry of Education, Culture, Sports, Science, and Technology of Japan through a Grant-in-Aid for Young Scientists (B) (Grant No. 17760151) and by the Japan Society for the Promotion of Science through a Grant-in-Aid for Scientific Research (Grants Nos. 17360085 and 17560740).

APPENDIX

The asymptotic growth rate for $N=2$ with $R_{10}\neq R_{20}$ is determined as follows: Assuming $\ddot{R}_j\approx 0$ and $R_j \gg R_{j0}$ ($j=1,2$), Eq. (3) reduces to

$$\left(\frac{3}{2}+\frac{R_1}{D}\right)\dot{R}_1^2=\frac{p_v-P_0-p_{\mathrm{ex}}}{\rho}-2R_2\left(\frac{1}{r_{12}}+\frac{1}{s_{12}}\right)\dot{R}_2^2, \tag{A1}$$

$$\left(\frac{3}{2}+\frac{R_2}{D}\right)\dot{R}_2^2=\frac{p_v-P_0-p_{\mathrm{ex}}}{\rho}-2R_1\left(\frac{1}{r_{12}}+\frac{1}{s_{12}}\right)\dot{R}_1^2. \tag{A2}$$

From these, we obtain

$$\dot{R}_1=\sqrt{\frac{p_v-P_0-p_{\mathrm{ex}}}{F\rho}}, \tag{A3}$$

$$F\equiv\frac{3}{2}+\frac{R_1}{D}+2\left(\frac{R_2}{r_{12}}+\frac{R_2}{s_{12}}\right)\frac{\left(\frac{3}{4}-\frac{R_1}{r_{12}}\right)+\left(\frac{R_1}{2D}-\frac{R_1}{s_{12}}\right)}{\left(\frac{3}{4}-\frac{R_2}{r_{12}}\right)+\left(\frac{R_2}{2D}-\frac{R_2}{s_{12}}\right)}, \tag{A4}$$

which is the time-dependent asymptotic growth rate of bubble 1, and gives the growth rate of bubble 2 by exchanging 1 and 2 in the subscripts. This reduces to Eq. (5) when $R_{10}=R_{20}$, and to Eq. (6) when the separation distances are infinitely large.

We make brief remarks on the magnitude of Eq. (A3). Since $s_{12}>2D$, and assuming $R_j\leqslant\frac{3}{4}r_{12}$, the last term of Eq. (A4) is positive, and the remaining terms in the same equation are always positive. Thus one knows that $F\geqslant\frac{3}{2}$, which means that the asymptotic growth rate in double-bubble cases (A3) is smaller than that in single-bubble cases not only when $R_{10}=R_{20}$ but also when $R_{10}\neq R_{20}$. Obviously Eq. (A3) is radius dependent as in the case of $R_{10}=R_{20}$.

[1] M. Futakawa, T. Naoe, C. C. Tsai, H. Kogawa, S. Ishikura, Y. Ikeda, H. Soyama, and H. Date, J. Nucl. Mater. **343**, 70 (2005).
[2] Y. Ikeda, J. Nucl. Mater. **343**, 7 (2005).
[3] J. R. Haines, B. W. Riemer, D. K. Felde, J. D. Hunn, S. J. Pawel, and C. C. Tsai, J. Nucl. Mater. **343**, 58 (2005).
[4] M. Futakawa, T. Naoe, H. Kogawa, C.-C. Tsai, and Y. Ikeda, J. Nucl. Sci. Technol. **40**, 895 (2003).
[5] B. W. Riemer, J. R. Haines, J. D. Hunn, D. C. Lousteau, T. J. McManamy, and C. C. Tsai, J. Nucl. Mater. **318**, 92 (2003).
[6] M. Futakawa, T. Wakui, H. Kogawa, and Y. Ikeda, Nucl. Instrum. Methods Phys. Res. A **562**, 676 (2006).
[7] T. Naoe, M. Futakawa, T. Koyama, and H. Kogawa, Jikken Rikigaku **6**, 301 (2006) (in Japanese).
[8] H. Kuttruff, Acustica **12**, 230 (1962); R. T. Smith, G. M. B. Webber, F. R. Young, and R. W. B. Stephens, Adv. Phys. **16**, 515 (1967). Cavitation and sonoluminescence in a variety of liquids, including liquid mercury, were studied.
[9] P. R. Williams, P. M. Williams, and S. W. J. Brown, J. Phys. D **31**, 1923 (1998). The tensile strength of liquid mercury was measured under pulsed dynamic stressing.
[10] M. Ida, Phys. Lett. A **297**, 210 (2002).
[11] M. Ida, Phys. Rev. E **67**, 056617 (2003).
[12] A. Ooi and R. Manasseh, ANZIAM J. **46**, C102 (2005).
[13] N. Bremond, M. Arora, C.-D. Ohl, and D. Lohse, Phys. Rev. Lett. **96**, 224501 (2006).
[14] A. A. Doinikov, Phys. Rev. E **64**, 026301 (2001).
[15] N. A. Pelekasis, A. Gaki, A. Doinikov, and J. A. Tsamopoulos, J. Fluid Mech. **500**, 313 (2004).
[16] M. Ida, Phys. Rev. E **72**, 036306 (2005).
[17] M. Ida, Phys. Fluids **17**, 097107 (2005).
[18] E. M. B. Payne, S. J. Illesinghe, A. Ooi, and R. Manasseh, J. Acoust. Soc. Am. **118**, 2841 (2005).
[19] J. R. Krieger and G. L. Chahine, J. Acoust. Soc. Am. **118**, 2961 (2005).
[20] C. E. Brennen, *Cavitation and Bubble Dynamics* (Oxford University Press, New York, 1995).